Research Article Vol. 5, No. 10 / October 2018 / Optica 1210

Sensitivity limits of millimeter-wave photonic radiometers based on efficient electro-optic upconverters

Gabriel Santamaría Botello,[1,†] Florian Sedlmeir,[2,†] Alfredo Rueda,[2,3,4,5,6] Kerlos Atia Abdalmalak,[1] Elliott R. Brown,[7] Gerd Leuchs,[2,8] Sascha Preu,[9] Daniel Segovia-Vargas,[1] Dmitry V. Strekalov,[10] Luis Enrique García Muñoz,[1,*] and Harald G. L. Schwefel[5,6]

[1]Universidad Carlos III de Madrid, Leganés, Spain
[2]Max Planck Institute for the Science of Light, Erlangen, Germany
[3]SAOT, School in Advanced Optical Technologies, Paul-Gordan-Str. 6, 91052 Erlangen, Germany
[4]Institute of Science and Technology Austria, am Campus 1, 3600 Klosterneuburg, Austria
[5]The Dodd-Walls Centre for Photonic and Quantum Technologies, New Zealand
[6]Department of Physics, University of Otago, Dunedin, New Zealand
[7]Wright State University, Dayton, Ohio 45435, USA
[8]Department of Physics, University of Erlangen-Nürnberg, Germany
[9]Technical University Darmstadt, Darmstadt, Germany
[10]Jet Propulsion Laboratory, California Institute of Technology, Pasadena, California 91125, USA
*Corresponding author: legarcia@ing.uc3m.es

Received 10 May 2018; revised 4 September 2018; accepted 5 September 2018 (Doc. ID 331440); published 1 October 2018

Conventional ultra-high sensitivity detectors in the millimeter-wave range are usually cooled as their own thermal noise at room temperature would mask the weak received radiation. The need for cryogenic systems increases the cost and complexity of the instruments, hindering the development of, among others, airborne and space applications. In this work, the nonlinear parametric upconversion of millimeter-wave radiation to the optical domain inside high-quality (Q) lithium niobate whispering-gallery mode (WGM) resonators is proposed for ultra-low noise detection. We experimentally demonstrate coherent upconversion of millimeter-wave signals to a 1550 nm telecom carrier, with a photon conversion efficiency surpassing the state-of-the-art by 2 orders of magnitude. Moreover, a theoretical model shows that the thermal equilibrium of counterpropagating WGMs is broken by overcoupling the millimeter-wave WGM, effectively cooling the upconverted mode and allowing ultra-low noise detection. By theoretically estimating the sensitivity of a correlation radiometer based on the presented scheme, it is found that room-temperature radiometers with better sensitivity than state-of-the-art high-electron-mobility transistor (HEMT)-based radiometers can be designed. This detection paradigm can be used to develop room-temperature instrumentation for radio astronomy, earth observation, planetary missions, and imaging systems.

OCIS codes: (190.0190) Nonlinear optics; (190.7220) Upconversion; (010.5630) Radiometry.

https://doi.org/10.1364/OPTICA.5.001210

1. INTRODUCTION

Detection of weak radiation at millimeter and submillimeter wavelengths is required for many applications of technological and scientific interest such as spectroscopy, imaging systems, earth observation, and planetary missions, as well as radio astronomy. As there is a particular motivation for studying the cosmic microwave background, galaxies, stars, and planetary systems at these wavelengths, future missions are currently being proposed and developed to retrieve unique information from this radiation [1–3]. Since the signals to be observed are usually weak compared to the thermal radiation generated by the receiver and its surroundings, ultra-low noise instrumentation is designed and placed inside cryostats to diminish the thermal noise contribution. This dramatically increases the size, cost, and complexity of instruments for airborne and space applications, while reducing the lifetime of the missions. In this paper we propose an alternative approach for designing flight-compatible receivers covering the millimeter-wave range that can eliminate or relax the cryogenic requirements: by passing the signal through a low-absorption nonlinear crystal pumped by a laser, the microwave photons are upconverted to the optical domain where detectors are less susceptible to thermal noise at room temperature.

Unlike conventional detectors, which are nearly perfect electromagnetic absorbers and thus ideal sources of thermal noise, the crystal is weakly coupled to the thermal bath by its low absorption and the low radiation losses of the mode. Hence, the microwave signal is upconverted to the optical domain before thermal noise populates the microwave mode. We show that with this novel paradigm, it is possible to realize a room-temperature detector whose noise performance approaches the quantum limit. For this, besides the need of a high-Q microwave structure that guarantees the decoupling to the environment, a highly efficient upconversion process is mandatory. We experimentally demonstrate nonlinear upconversion of 80 GHz signals to a 194 THz carrier inside a high-Q lithium niobate whispering-gallery mode (WGM) resonator, showing 2 orders of magnitude higher efficiency than the best reported so far [4]. The paper is structured as follows. In Section 2, we discuss the WGM-based upconverter and analyze its thermal noise contribution and conversion efficiency. In Section 3, the performance of the proposed detector as a radiometer is estimated and compared to conventional technology. We follow an approach where background thermal noise cancellation is done at room temperature by cross-correlation in the optical domain. In Section 4, the experimental setup of a WGM-based upconverter is explained and results are shown. Finally, conclusions are given in Section 5.

2. ELECTRO-OPTIC UPCONVERTER

In a conventional microwave receiver, noise originates from different sources with thermal noise being the dominant one due to the low energy of microwave photons. While microwave photons are completely masked by thermal noise if they are directly detected at room temperature, upconversion into the optical domain boosts the photon energy, allowing for room temperature detection with commercially available devices. It is challenging though to achieve a high photon conversion efficiency η, defined as the ratio of the numbers of output optical and input microwave photons. This is so because in optically transparent materials even the strongest second-order susceptibilities $\chi^{(2)}$ are only on the order of a few pm/V. This leads to weak interactions unless extremely high field intensities are applied. Using a high-power optical pump entails a series of technical complications, such as, e.g., excessive noise and a very strong pump suppression requirement. These limitations have so far precluded any practical realization of the upconversion approach. The field enhancement in high-Q WGM resonators made of nonlinear crystals helps to solve these problems, leading to the state-of-the-art efficiencies on the order of $\eta \approx 10^{-7}$ per 1 mW continuous wave (CW) pump power, for millimeter-wave signals [4,5] (in the small signal regime, η scales proportionally with the pump power). WGM cavities trap light by propagation along the resonator rim such that the light constructively interferes with itself to build up a resonance. Therefore, microwave and optical pump modes at frequencies ν and ν_p, respectively, can be trapped in the same region of space, allowing for high modal overlap and strong nonlinear coupling via the second-order response $\chi^{(2)}$ of the material's polarization. In general, this interaction generates multiple optical sidebands, but the resonator can be optimized to resonate only at the sideband produced by sum frequency generation (SFG) and/or difference frequency generation (DFG) processes [6]. The SFG process is preferred since it is free of spontaneous parametric down conversion (SPDC) noise [7,8]. Thus, an optical sideband at frequency $\nu_s = \nu + \nu_p$ is generated inside the resonator and then outcoupled and detected at room temperature with a photonic detector. Since the SFG process is coherent and noiseless, the sideband contains all the information from the microwave signal provided that 100% of photons are upconverted. This scheme is depicted in Fig. 1 where a prism is used for incoupling of the pump and outcoupling of the sideband. A dielectric rod waveguide is coupled to the antenna (for example, a horn) and to the resonator via the near evanescent field.

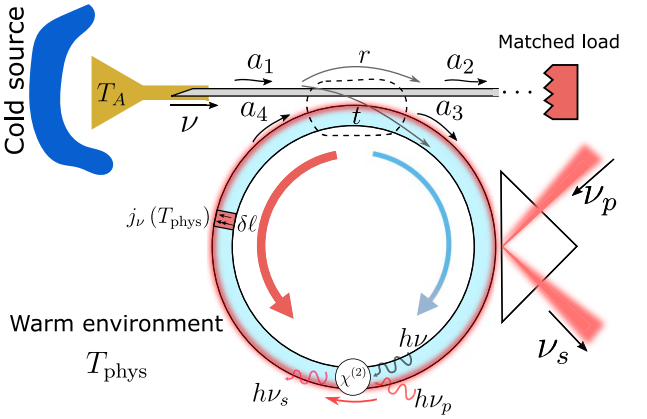

Fig. 1. Coupling of millimeter-wave and optical radiation to the WGM resonator. The microwave coupling region (enclosed by the dashed curve) is considered small and lossless. Input and output modes in the waveguide and the resonator are defined with normalized field amplitudes $a_i(\nu)$ such that their squared norm equals the power spectral density of the mode. The coupling system can be viewed as a four-port network whose scattering matrix is characterized by the waveguide's reflection coefficient $r = a_2/a_1$ and waveguide-resonator transmission coefficient $t = a_3/a_1$. The cavity's reflection coefficient $r' = a_3/a_4$ and cavity-waveguide transmission coefficient $t' = a_2/a_4$ have the same magnitudes as r and t, respectively, but a different phase in general.

A. Conversion Efficiency

In a general nonlinear interaction scheme with undepleted pump and microwave modes (small signal regime), the photon-number upconversion efficiency η scales linearly with the microwave and pump total power, and quadratically with the second-order susceptibility $\chi^{(2)}$, the modal overlap, and the interaction length [9]. In a WGM resonator, the power enhancement of optical and microwave modes (ratio between intracavity and input power) is proportional to the quotient between the corresponding quality factor and the resonator's radius. If the pump is monochromatic and critically coupled, the conversion efficiency of a broadband microwave signal is given by [6,10]

$$\eta = P_p Q_p Q_s \frac{g^2}{\pi \hbar \nu_p^2 \nu_s} \left(\frac{Q_s}{Q_s^c}\right) \tau F, \tag{1}$$

where τ is the roundtrip time of the microwave WGM, F is the microwave power enhancement, P_p is the input pump power, Q_p and Q_s are the loaded quality factor of the pump and sideband, respectively, and Q_s^c is the sideband's coupling quality factor. The ratio $Q_s/Q_s^c = 1/2$ for a critically coupled sideband and approaches 1 when it is overcoupled. The nonlinear coupling rate g takes into account the modal overlap and is given by [6]

$$g = \chi^{(2)}\zeta \frac{\int_V \Psi_p \Psi \Psi_s^* \, dV}{\sqrt{\int_V |\Psi_p|^2 \, dV \int_V |\Psi|^2 \, dV \int_V |\Psi_s|^2 \, dV}}, \quad (2)$$

where Ψ_p, Ψ, and Ψ_s are the pump, microwave, and sideband mode distribution, respectively, and $\zeta = 4\pi\varepsilon_0(\hbar/8)^{1/2}(\nu_p\nu_s\nu)^{1/2}/(\varepsilon_p\varepsilon_s\varepsilon)^{1/2}$ with ε_p, ε, and ε_s being the pump, microwave, and sideband permittivities of the media, respectively. The integration takes place over the infinite space volume V. From the theoretical models of the conversion efficiency and with the aid of full-wave microwave and optical simulations, optimal upconverters can be designed and then characterized experimentally.

B. Thermal Occupation

A room-temperature receiver intended to work as a radiometer measures the mean power coming from a thermal source, which is in general much colder than the physical temperature of the detector. Therefore, an important challenge is the reduction of the thermal noise coupled to the resonator when operating at room temperature, since this noise will be upconverted to the optical domain along with the signal coming from the source. Interestingly, the resonator can be overcoupled to the antenna that is pointing to the cold source, radiatively cooling the thermally populated microwave modes given the low dissipation of the crystal and thus reducing significantly the noise temperature of the receiver [11]. This is a subtle point that deserves a more detailed explanation. Consider the schematic in Fig. 1, where the microwave signal from the cold source propagates in a waveguide from left to right. It couples to a *clockwise* propagating WGM. Thermal radiation outcoupled from this mode continues to propagate toward the right end of the waveguide. That end can be "hot," leading to strong thermal radiation propagating to the left. However, this radiation couples to a different, *counterclockwise* propagating mode. In this sense, the directional thermal equilibrium in the system is broken, and the "hot" right end of the waveguide serves as a perfect zero-temperature cooler for the clockwise propagating mode. Superficially, this situation resembles the Maxwell's demon mischief; however, it is not the case, since we deal with a nonequilibrium system driven by the temperature difference between the hot resonator and the cold thermal source. Hence, due to strict phase-matching conditions, upconversion of a single microwave mode—the clockwise one that is coupled to the cold source—can be engineered [5], reducing the upconverted thermal noise arising from the converter itself. From this, we can find the ultimate sensitivity of a strongly overcoupled room temperature radiometer based on high efficiency microwave-to-optical upconversion inside WGM cavities. If the resonator has a physical temperature T_{phys}, it will generate thermal noise that will be upconverted along with the microwave signal coupled from the antenna. To analyze such thermal contribution, consider Fig. 1. The temperature T_A of the mode coupled to the antenna is equivalent to the temperature of the black body source that covers the entire angular radiation width of the antenna. This is a consequence of the λ^2 proportionality of the antenna's aperture and the $1/\lambda^2$ dependence of the black body's brightness, λ being the radiation wavelength [12]. The microwave field propagates through the waveguide and couples partially to the resonator mode while the remaining power keeps propagating in the waveguide. The mode coupling and waveguide transmission of the incident field are described by complex coefficients t and r, respectively. The resonator has a field dissipation coefficient α, such that in one roundtrip the power of the microwave WGM is attenuated by a factor $a^2 = \exp(-2\alpha L)$, L being the roundtrip length. From these coefficients, the well-known Fabry–Perot equations for the intracavity and reflected power can be obtained [13],

$$|a_4(\nu)|^2 = \frac{a^2(1-|r|^2)}{|1-a|r|\exp(i2\pi\tau\delta\nu)|^2}|a_1(\nu)|^2, \quad (3)$$

$$|a_2(\nu)|^2 = \left[1 - \frac{(1-|r|^2)(1-a^2)}{|1-a|r|\exp(i2\pi\tau\delta\nu)|^2}\right]|a_1(\nu)|^2, \quad (4)$$

where $\delta\nu = \nu - \nu_0$, ν_0 being the resonance frequency. According to Fig. 1, the mode amplitudes $a_i(\nu)$ are normalized such that $|a_i(\nu)|^2 = \lim_{\Delta t\to\infty}\frac{1}{\Delta t}\langle|a_i'(\nu)|^2\rangle$ gives the power spectral density of the mode (a_i' is the Fourier transform of the time-domain mode as truncated over the interval Δt, and $\langle\cdot\rangle$ denotes ensemble average).

Consider the scenario where $T_A = T_{\text{phys}}$ and the waveguide ends in a matched load also at temperature T_{phys}. The whole system is in thermal equilibrium, and the net power spectral density flow must be zero everywhere. However, a fraction $1-\exp(-2\alpha\delta\ell)$ of the power traveling inside the resonator is dissipated over a distance $\delta\ell$. To keep thermal equilibrium, i.e., the power of the thermal mode remains constant under propagation, this loss must be compensated by a point thermal source producing a power spectral density [14],

$$|j_\nu(T_{\text{phys}})|^2 = h\nu(1-\exp(-2\alpha\delta\ell))\Theta_\nu(T_{\text{phys}}), \quad (5)$$

where

$$\Theta_\nu(T) = [\exp(h\nu/(k_B T)) - 1]^{-1}, \quad (6)$$

is the Planck function with h and k_B the Planck and Boltzmann constants, respectively. The emergence of electromagnetic sources inside the resonator has also a physical justification outside it: it is expected that due to the presence of the cavity, the waveguide's transmitted power decreases near resonance frequencies, apparently breaking thermal equilibrium. Indeed, for critical coupling $|r| = a$, this transmission is totally canceled at a resonant frequency [13]. Since we assumed thermal equilibrium, and the waveguide's matched load propagates black body radiation towards the resonator, some thermal radiation generated within the cavity must leak through the waveguide to compensate for the transmission suppression and to guarantee zero net power transfer along the waveguide. Thus, dips in the transmission spectrum can only be observed if $T_{\text{phys}} < T_A$, in which case the system is not in thermal equilibrium.

A source $j_\nu(T_{\text{phys}})$ at point ℓ_1 of the resonator's perimeter will produce a response $b_\nu(\ell_2,\ell_1)$ at point ℓ_2 that accounts for the infinite roundtrips of the field within the resonator and is given by

$$|b_\nu(\ell_2,\ell_1)|^2 = \frac{K(\ell_2,\ell_1)}{|1-a|r|\exp(i2\pi\tau\delta\nu)|^2}|j_\nu(T_{\text{phys}})|^2, \quad (7)$$

where

$$K(\ell_1,\ell_2) = \begin{cases} \exp[-2\alpha(\ell_2-\ell_1)] & \ell_2 \geq \ell_1 \\ |r|^2\exp[-2\alpha(L+\ell_2-\ell_1)] & \ell_2 < \ell_1 \end{cases}. \quad (8)$$

The contribution of the uncorrelated continuum of sources $j_\nu(T_{\text{phys}})$ as $\delta\ell \to 0$ is obtained from integration of Eq. (7) over the resonator's perimeter $\int_0^L |b_\nu(\ell_2,\ell_1)|^2 \, d\ell_1$ resulting in

$$|s_n(\nu,\ell_2)|^2 = \frac{1-|r|^2a^2-(1-|r|^2)a^{2\ell_2/L}}{|1-ar\exp(i2\pi\tau\delta\nu)|^2}h\nu\Theta_\nu(T_p), \quad (9)$$

which is at the end dependent on the observation point ℓ_2. The thermal noise source inside the cavity $j_\nu(T_{\text{phys}})$ depends only on the resonator's losses and physical temperature, so it remains unchanged even when the resonator is not in thermal equilibrium with the antenna [14]. Therefore, we can study independently the thermal contributions of the "hot" resonator mode and the "cold" waveguide mode coupled to the antenna pointing to a cold source at temperature T_A. It can be seen from Eq. (9) that the noise contribution of the cavity is minimum at $\ell_2 = 0$ and maximum at $\ell_2 = L$. This makes sense since the resonator mode is cooled at the point of contact with the "cold" waveguide mode ($\ell_2 = 0$). As the field propagates within the resonator, the mode is heated at a rate α due to the lossy medium. On the other hand, the field from the waveguide, attenuates as propagates inside the cavity with the same rate α, yielding Eq. (3) at $\ell_2 = L$. Hence, the total spatially dependent contribution to the mode in the resonator is

$$|s_T(\nu,\ell_2)|^2 = \underbrace{\frac{a^{2\ell_2/L}(1-|r|^2)}{|1-a|r|\exp(i2\pi\tau\delta\nu)|^2}h\nu\Theta_\nu(T_A)}_{\text{Antenna contribution}} + \underbrace{\frac{1-|r|^2a^2-(1-|r|^2)a^{2\ell_2/L}}{|1-a|r|\exp(i2\pi\tau\delta\nu)|^2}h\nu\Theta_\nu(T_{\text{phys}})}_{\text{"Hot" resonator contribution}}, \quad (10)$$

since the thermal sources are uncorrelated. This microwave power spectral density is upconverted to the optical domain with an efficiency proportional to total intracavity energy, as seen from the term τF in Eq. (1). Thus, the power spectral density of the upconverted radiation will be proportional to $\int_0^L |s_T(\nu)|^2\, d\ell_2$. Substituting Eq. (10), we get a total upconverted power P_s, which scales as

$$P_s \propto \frac{(1-a^2)(1-|r|^2)}{\ln(a^{-2})}h\nu[\Theta_\nu(T_A)+\Theta_\nu(T_{\text{eff}})], \quad (11)$$

where

$$\Theta_\nu(T_{\text{eff}}) = \left[\frac{(1-a^2|r|^2)\ln(a^{-2})}{(1-a^2)(1-|r|^2)}-1\right]\Theta_\nu(T_{\text{phys}}). \quad (12)$$

This means we can think about a noiseless (lossless) resonator and model the actual thermal contribution of it as an additional source of noise at the input of the antenna, whose power spectral density is that of a black body at an effective temperature T_{eff}. In the Rayleigh–Jeans region this is

$$T_{\text{eff}} = \left[\frac{(1-a^2|r|^2)\ln(a^{-2})}{(1-a^2)(1-|r|^2)}-1\right]T_{\text{phys}}. \quad (13)$$

T_{eff} should not be confused with the temperature of the thermal radiation circulating in the resonator mode as this might be indeed higher due to the microwave power enhancement. It is instead the temperature of a fictitious "heater" added to the input of the antenna to take into account the intrinsic thermal noise of the resonator. Provided that the resonator has low losses $a \approx 1$ and is strongly overcoupled $|r| \ll a$, T_{eff} can be significantly lower than the temperature of the environment, reaching the theoretical limit $[\ln(a^{-2})/(1-a^2)-1]\,T_{\text{phys}}$ at $r = 0$ when there is no intracavity microwave field enhancement.

3. RADIOMETER CONCEPT

A radiometer measures the electromagnetic energy collected—normally from a thermal source—by an antenna during a period Δt, such that the power average, and thus temperature of the source, can be estimated. From the quantum point of view, an ideal radiometer does not add noise and is capable of counting individual photons with 100% efficiency at a frequency ν over a bandwidth $\Delta\nu$. Even though this hypothetical radiometer has the highest achievable sensitivity, the power measurement during a finite observation time carries an uncertainty due to the randomness of the thermal source. While photons naturally arrive at random times (shot noise), the intensity of the source exhibits also Gaussian fluctuations due to its thermal nature. This leads to the well-known super Poissonian statistics [15] in the number of photon counts during an interval Δt. The fluctuations—standard deviation—in the photon counts Δn can be calculated from the Mandel formula [15,16], which for observation times much longer than the coherence time $\Delta t \gg 1/\Delta\nu$ yields

$$\Delta n = \sqrt{\bar{n}+\frac{(\bar{n})^2}{\Delta\nu\Delta t}}, \quad (14)$$

where $\bar{n} = \Theta_\nu(T_A)\Delta\nu\Delta t$ is the expected value of the photon counts. We have assumed T_A to be the temperature of the thermal source being observed. The first term in the square root of Eq. (14) reflects the Poissonian distribution of photon arrival (shot noise) whereas the second term accounts for the Gaussian fluctuations of the source. The fluctuation Δn can be translated into a temperature uncertainty ΔT by taking the inverse Planck function, establishing the so-called quantum limit of a radiometer. As expected, the sensitivity increases with the bandwidth-time product since more information is obtained from the source.

In a real radiometer, while some photons are lost due to its imperfect efficiency <100%, noise is created from different sources (mainly thermal noise due to the nonzero physical temperature of the radiometer). Although upconversion of microwave signals with low thermal noise contribution is possible as discussed in Section 2, a radiometer requires an integration technique that increases its sensitivity by observing the source for longer periods. Such an integration technique can be designed to reduce the thermal contribution of the radiometer with the observation time. For instance, Dicke-switching schemes [12] alternately switch the radiometer's input between the source and a calibrated black body reference. Then, with a lock-in detection scheme, the thermal noise generated by the receiver can be estimated and canceled from the measurement. Another possibility is a cross-correlation scheme, where the outputs of two detectors measuring the same source are cross-correlated. Since thermal noise generated within the detectors is uncorrelated, the output converges to the source power without noise. Besides noise cancellation, this approach can also be used for interferometry provided that each upconverter is coupled to its own antenna [17,18]. This scheme is advantageous for room temperature operation since no black body reference is required. Moreover, the proposed upconversion scheme is coherent and thus suitable for realizing cross-correlation in the optical domain with low losses. Figure 2 shows an interferometry with cross-correlation scheme, where the radiation from a source at temperature T_A is collected by two antennas pointing to the same direction and sent to two

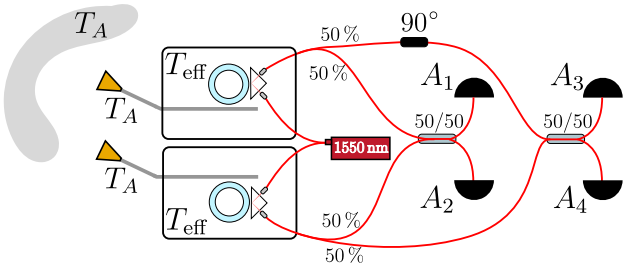

Fig. 2. Upconversion based cross-correlation interferometer receiver. The antennas feed two upconverters with effective noise temperature T_{eff} and efficiency η. The upconverted signals are cross-correlated in two stages, to retrieve the autocorrelation of the in-phase and quadrature signals.

WGM resonators acting as upconverters with efficiency η. Each upconverter generates noise at the equivalent temperature T_{eff} due to its physical temperature. Even though each antenna is coupled to a slightly different spatial mode, both band-limited signals are strongly correlated provided that the detection coherence time is much longer than the delay between the radiation received by the antennas,

$$1/\Delta\nu \gg d \sin\theta_0/c, \tag{15}$$

with θ_0 the antenna's half-beamwidth, d the antenna separation, and c the speed of light. This is a consequence of the Van Cittert–Zernike theorem, which states that the cross-correlation $\Gamma = \langle s_1(\boldsymbol{P}_1, t) s_2^*(\boldsymbol{P}_2, t)\rangle$ between signals s_1 and s_2 received by two antennas at different points in the xy plane $\boldsymbol{P}_1$ and $\boldsymbol{P}_2$ is proportional to the Fourier transform of the observed angular brightness of the uncorrelated source [19],

$$\Gamma \propto \iint B(l_x, l_y) F^2(l_x, l_y) \exp[-i2\pi(ul_x + vl_y)] \mathrm{d}l_x \mathrm{d}l_y, \tag{16}$$

where in spherical coordinates, $l_x = \sin\theta\cos\phi$ and $l_y = \sin\theta\sin\phi$ are the direction cosines of the vector directed to the source (assuming the antennas are pointing in the z direction), $B(l_x, l_y)$ is the brightness of the source, $F^2(l_x, l_y)$ is the power radiation pattern of the antennas, and (u, v) are the λ-normalized coordinates of $\boldsymbol{P}_2 - \boldsymbol{P}_1$. This Fourier pair determines the ranges of separation between antennas that guarantee the coherence between received band-limited signals. Hence, narrower antenna beamwidths yield larger minimum separation distances d that keep coherence. Nevertheless, despite the fulfillment of Eq. (15), the phase of the carrier will be different at each antenna, resulting in received signals with the phasor representations $s_1(t) \propto a(t)\exp(i2\pi\nu t)$ and $s_2(t) \propto a(t)\exp(i2\pi\nu t)\exp(i\phi)$, where $a(t)$ is the band-limited signal envelope and ϕ the phase shift between carriers. For this reason, in Fig. 2 two parallel stages measure the cross-correlation between the generated sidebands. The first one with photodiodes A_1 and A_2 correlates the sidebands generated by each upconverter by interfering them in a 50/50 beamsplitter and then detecting the outputs with the balanced photodiodes. If $\phi = 0$, the beamsplitter cancels the antenna signal in the output detected by A_2 due to destructive interference. Thus, A_2 will count only noise photons generated by the upconverters providing the baseline calibration, whereas A_1 will additionally count those from the source. Since the noise generated by each upconverter is uncorrelated, the difference between photon counts will converge to the power of the source. For an arbitrary carrier phase mismatch ϕ, A_1 and A_2 count on average

$$\overline{n_1} = \frac{\eta\Delta\nu\Delta t}{2}[\Theta_\nu(T_{\text{eff}}) + (1 + \cos\phi)\Theta_\nu(T_A)], \tag{17}$$

$$\overline{n_2} = \frac{\eta\Delta\nu\Delta t}{2}[\Theta_\nu(T_{\text{eff}}) + (1 - \cos\phi)\Theta_\nu(T_A)] \tag{18}$$

photons, respectively, during the interval Δt. The difference between photon counts converges then to $\overline{n_1} - \overline{n_2} = \cos\phi\eta\Delta\nu\Delta t\Theta_\nu(T_A)$. Similarly, the second cross-correlation stage with A_3 and A_4 converges to $\overline{n_4} - \overline{n_3} = \sin\phi\eta\Delta\nu\Delta t\Theta_\nu(T_A)$ due to the $\pi/2$ phase delay applied to one of the upconverter's output. The statistical averages $\overline{n_3}$ and $\overline{n_4}$ have the same form as Eqs. (18) and (17), respectively, after replacing $\cos\phi$ by $\sin\phi$. The temperature of the source can thus be retrieved from the squares of the differences measured $n_T = [(n_4 - n_3)^2 + (n_1 - n_2)^2]^{1/2}$. The random variables n_i have Bose–Einstein distribution for $\Delta t\Delta\nu \ll 1$ and approximate the Poisson distribution for $\Delta t\Delta\nu \gg 1$. However, for arbitrary values of Δt, the distribution has in general no analytical solution [15]. Nevertheless, the variance of the photon count differences can be approximated as $\mathrm{Var}[n_i - n_j] = \mathrm{Var}[n_i] + \mathrm{Var}[n_j]$ as the covariance between n_i and n_j vanishes for long integration times $\Delta t \gg 1/\Delta\nu$. This is a consequence of the unity second-order coherence $g^{(2)}(0) \approx 1$ observed in the Brown–Twiss interferometer for integration times much longer than the coherence time [15]. Then, a first-order Taylor expansion of n_T is used to estimate $\overline{n_T} \approx \eta\Delta\nu\Delta t\Theta_\nu(T_A)$ and $\mathrm{Var}[n_T] \approx \cos^2\phi\mathrm{Var}[n_1 - n_2] + \sin^2\phi\mathrm{Var}[n_4 - n_3]$ as the covariances vanish. $\mathrm{Var}[n_T]$ determines the measurement uncertainty of the radiometer. Finding the variances $\mathrm{Var}[n_i]$ from Eq. (14), the standard deviation in the measurement Δn_T results in

$$\frac{\Delta n_T}{\eta\Delta\nu\Delta t} = \left[\frac{\Phi_\nu + \eta\Phi_\nu^2 + \eta(\cos^4\phi + \sin^4\phi)\Theta_\nu^2(T_A)}{\eta\Delta\nu\Delta t}\right]^{1/2}, \tag{19}$$

where we have abbreviated $\Phi_\nu = \Theta_\nu(T_{\text{eff}}) + \Theta_\nu(T_A)$. Equation (19) can be expressed as a temperature uncertainty ΔT from the inverse of the Planck function,

$$T_A + \Delta T = \frac{h\nu}{k_B \ln\left[1 + \left(\Theta_\nu(T_A) + \frac{\Delta n_T}{\eta\Delta\nu\Delta t}\right)^{-1}\right]}, \tag{20}$$

yielding the rms error in the temperature measurement. This sets the ultimate sensitivity of the receiver since multiple observations under identical conditions would produce different results whose statistical mean is the actual temperature of the source and whose standard deviation is ΔT. In the Rayleigh–Jeans region, and for $T_A \ll T_{\text{eff}}$, the temperature uncertainty converges to $\Delta T \approx (T_{\text{eff}} + T_A)/(\Delta\nu\Delta t)^{1/2}$. For highly directive antennas, the phase mismatch $\phi \to 0$ and the second cross-correlation stage with A_3 and A_4 can be dropped. In such a case, the radiometer is $\sqrt{2}$ times more sensitive, with a Rayleigh–Jeans uncertainty of $\Delta T \approx (T_{\text{eff}} + T_A)/(2\cos^2\phi\Delta\nu\Delta t)^{1/2}$ as expected from a single-stage correlation interferometer scheme [12].

Figure 3 shows the theoretical normalized temperature uncertainty of the conceptual radiometer $\Delta T\sqrt{\Delta\nu\Delta t}$ as a function of T_{eff} and parametrized by ν and η, all according to Eq. (20). The observation of a cold source such as the cosmic microwave background ($T_A \approx 2.7$ K) was assumed. The sensitivity results

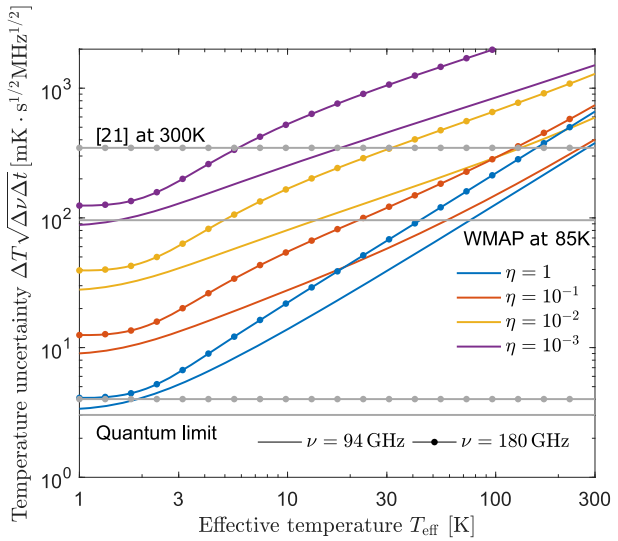

Fig. 3. Normalized temperature uncertainty of the upconversion-based radiometer obtained from Eq. (20). For 100% efficient upconversion, the curves converge to the quantum limit derived from Eq. (14) as $T_{\text{eff}} \to 0$. All curves converge to a linear function of T_{eff} when Gaussian noise of the CMB dominates over shot noise as $T_{\text{eff}} \to \infty$. Shot noise starts to dominate for low temperatures T_{eff}, causing a deviation of the curves from the linear behavior and preventing vanishing uncertainties.

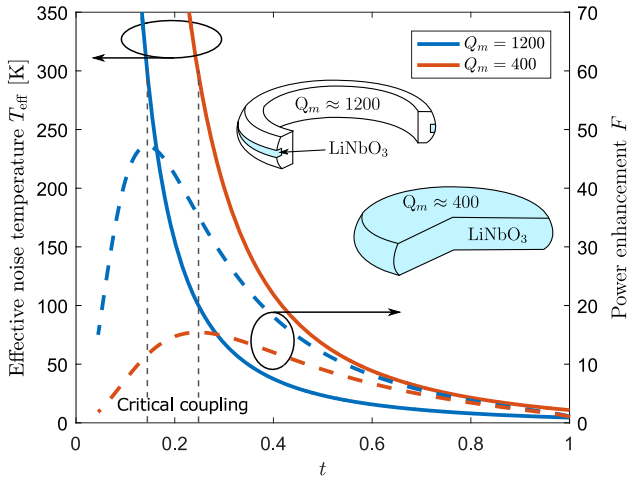

Fig. 4. Effective noise temperature and millimeter-wave power enhancement of two resonators coupled to a waveguide with different strength $|t| = \sqrt{1-|r|^2}$: a lithium niobate disk with an intrinsic millimeter-wave $Q \approx 400$ and a thin lithium niobate ring surrounded by a low-loss medium such as sapphire, with $Q \approx 1200$. Vertical-dashed lines represent the critical coupling point for each resonator, at which the intracavity power enhancement is maximum and $T_{\text{eff}} \approx T_{\text{phys}}$. An azimuthal mode number $m = 4$ and $T_{\text{phys}} = 300$ K are considered.

are plotted for two different frequencies $\nu = 94$ GHz and $\nu = 180$ GHz and compared to those of the Wilkinson microwave anisotropy probe (WMAP) design [20] (a radio astronomy benchmark) as well as the state-of-the-art room-temperature HEMT MMIC low-noise amplifiers [21]. WMAP radiometers are also based on HEMT low-noise amplifiers that are passively cooled down to physical temperatures of about 85 K. As a comparative example, it can be seen that the same sensitivity as in WMAP W-band LNAs could be achieved for $\eta = 10^{-2}$ and $T_{\text{eff}} = 14$ K. From Eq. (13), such equivalent temperature is achievable in millimeter-sized disc-shaped $LiNbO_3$ resonators cooled down to 85 K, excited with an azimuthal mode number $m = 4$ and overcoupled such that $|t| \simeq 0.57$. At these frequencies the resonator can exhibit an intrinsic $Q \approx 400$, yielding a roundtrip attenuation factor $a^2 = \exp(-2\pi m/Q) \simeq 0.94$ and a microwave enhancement $F = a^2(1-|r|^2)/(1-a|r|)^2 \simeq 7$ (see Fig. 4). Nevertheless, the same sensitivity can also be achieved at room temperature if higher microwave quality factors on the order of $Q \approx 1200$ are realized in μm-thick and millimeter-radius $LiNbO_3$ rings, partially surrounded by a thicker ring of low-loss materials such as sapphire or high-resistivity silicon to sustain the mode. In this case, for a mode $m = 4$ the roundtrip attenuation factor results $a^2 \simeq 0.98$, and the power enhancement $F \simeq 8$ when overcoupling with coefficient $|t| \simeq 0.6$. At this point, the significant increase in the temperature uncertainty for lower efficiencies evidenced in Fig. 3 proves the domination of the shot noise: For an efficiency $\eta = 5 \times 10^{-2}$, the effective temperature requirement to match WMAP sensitivity relaxes to $T_{\text{eff}} = 45$ K. This can be achieved with the same cavity and mode if $|t| = 0.36$, corresponding to $F \approx 22$. On the other hand, at 180 GHz and under the $\eta \approx 10^{-2}$ and $T_{\text{eff}} \approx 14$ K conditions, the radiometer would exhibit a Rayleigh–Jeans system temperature of 211 K in contrast to the 346.7 K of [21]. Increasing further the efficiency up to $\eta = 0.1$ would lead to system temperatures as low as 70 K. Interestingly, there is no fundamental mechanism besides the quantum limit, upon which the sensitivity of a highly efficient upconverter degrades at higher frequencies, provided that high millimeter-wave intrinsic Q factors are achieved. Indeed, higher frequencies improve the modal overlap between microwave and optical modes, thus increasing the photon conversion efficiency.

One of the advantages of the cross-correlation radiometers is their insensitivity to gain fluctuations in the receivers [12]. In our case, efficiency variations arise in the upconverters of Fig. 2 due to fluctuations in the instantaneous pump power, produced by the relative intensity noise (RIN) of the laser. As the conversion efficiency is proportional to the intracavity pump power, high-frequency components of RIN (higher than the resonator's optical linewidth) are low-pass filtered by the high-Q resonator. Moreover, RIN fluctuations faster than $1/\Delta t$ will be reduced due to averaging over the integration time of the radiometer. Accounting for RIN, the efficiency η in Eqs. (17) and (18) is replaced by $\bar{\eta}(1 + \delta P_{\text{int}}/P_{\text{int}})$, where $\bar{\eta}$ is the mean efficiency, and $\delta P_{\text{int}}/P_{\text{int}}$ the instantaneous zero-mean relative intracavity pump power fluctuations averaged during the integration time Δt. This leads to fluctuations in the power measured by each photodetector, but only those added to the signal from the antenna remain significant after taking the difference between photon counts. In the Rayleigh–Jeans region, the new temperature uncertainty $\Delta T'$ taking into consideration the laser's RIN is bounded as

$$\Delta T' \le \Delta T\sqrt{1 + \frac{\delta P_{\text{int}}}{P_{\text{int}}}} + T_A\frac{\delta P_{\text{int}}}{P_{\text{int}}}, \tag{21}$$

where ΔT is the RIN-free temperature uncertainty calculated as in Eq. (20). Averaging over Δt the time-domain relative power fluctuation whose rms value RIM_{rms} is a specification of the laser, then $\delta P_{\text{int}}/P_{\text{int}} = (\Delta\nu_p\Delta t)^{-1/4}\text{RIN}_{\text{rms}}$ where $\Delta\nu_p$ is the resonator's optical linewidth. Assuming a reasonable laser RIN value

$\mathrm{RIN}_{\mathrm{rms}} = 10^{-4}$ up to $\Delta\nu_p = 2$ MHz, and an integration time $\Delta t = 1$ s, the laser contribution to the temperature uncertainty is below $(2.66 \times 10^{-6})\,T_A$, which is negligible compared to the ΔT levels discussed from Fig. 3 for arbitrarily large detection bandwidths $\Delta\nu$. Overall, RIN contribution is small (less than 15.2 mK $s^{1/2}$ $MHz^{1/2}$) even for large detection bandwidths and integration times up to $\Delta\nu = 10$ GHz and $\Delta t = 10^5$ s, respectively. Nevertheless, the effect of RIN on the receiver's temperature can in principle be reduced further by monitoring the instantaneous laser power and correcting the photodetected measurements in a postprocessing stage. Feed-forward control schemes can also be used to decrease intensity noise.

Drifts in the laser's wavelength do not affect the millimeter-wave upconversion frequency as this depends on the free-spectral range of the resonator. However, a narrow linewidth laser locked to the cavity mode is needed to reduce the intracavity power (and, thus, efficiency) fluctuations due to mode detuning. For a Lorentzian-shaped cavity mode of ≈2 MHz width, the effect of a ≤50 kHz linewidth laser on the sensitivity degradation is negligible, being on the order of the effect of laser RIN as discussed above.

4. UPCONVERSION EXPERIMENT

We have tested a proof-of-concept 80 GHz upconverter whose experimental setup is shown in Fig. 5. A photomixing setup is used as the microwave emitter, wherein two telecom lasers detuned by the microwave frequency are combined. The beat note is amplified to feed a photomixer [22] that radiates at the microwave frequency through a gallium arsenide (GaAs) rod waveguide [23] that is coupled to a 5.66 mm diameter z-cut lithium niobate ($LiNbO_3$) WGM resonator. A second photomixer is fed with the same optical beat note and acts as a microwave receiver allowing the measurement of the microwave spectrum of the cavity. A diamond prism mounted on a piezo stage couples a 1550 nm laser beam focused with a GRIN lens to the same WGM cavity. The light emitted from a narrowband (<100 KHz) telecom laser is polarized and passed through an amplified spontaneous emission (ASE) filter to reduce the noise floor level. An electro-optic modulator is used for locking the laser to a resonator mode employing the Pound–Drever–Hall scheme, such that temperature stabilization is not needed.

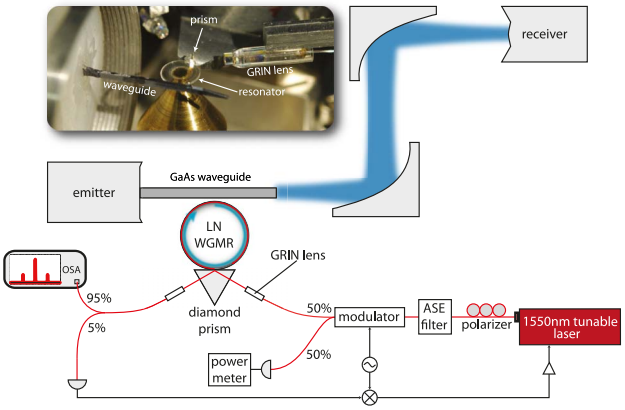

Fig. 5. Nonlinear upconversion experimental setup, showing the WGM cavity excited with resonant microwave and optical modes coupled by a dielectric rod waveguide and a prism, respectively.

The upconverted signal coming from the resonator and the reflected part of the pump are coupled to a fiber via a second GRIN lens and guided to the optical spectrum analyzer and a photodiode for sideband characterization and spectrum measurement, respectively. The resulting optical and microwave coupling efficiencies are about 50% and 90%, respectively. Optical resonances with free spectral range of FSR = 7.883 GHz and 2.45 MHz of bandwidth were observed. This corresponds to an intrinsic Q factor around 1.6×10^8. The microwave mode had azimuthal order $m = 10$, an intrinsic Q factor of about 400 and a power enhancement $F \approx 6$ when critically coupled.

The cavity is designed to phase-match the nonlinear interaction; i.e., all WGMs must have the same phase velocity. For fundamental WGMs, this constrains the microwave, pump, and upconverted sideband modes to have azimuthal mode numbers m, m_p, and m_s, respectively, that fulfill the relations $m_s = m_p + m$ or $m_s = m_p - m$ for SFG and DFG processes respectively, in order to ensure that the overlap integral of Eq. (2) does not vanish. This implies that the microwave frequency must satisfy $\nu = m \times \mathrm{FSR}$, where FSR is the optical free spectral range. Owing to the fabrication and full-wave simulations' limited accuracy, the resonator size had to be fine-tuned by several polishing steps to actually achieve the phase-matching. Figure 6 depicts the results of this process: the optical FSR and the microwave resonance frequency decrease with the resonator's radius with different slopes. The radius has been calculated from the measured FSR using the theoretical dispersion curve of the optical mode [24]; therefore, each measured point lies exactly on the theoretical curve. The dispersion of the microwave mode is expected to be approximately linear with the radius as well. However, uncertainty in the measured microwave frequency and slightly different coupling conditions in each measurement contribute to the deviations of the microwave dispersion curve. Approximate fulfillment of the phase-matching condition was found at 79 GHz, corresponding to $R = 2.83$ mm. At this point, upconversion takes place for the slightly detuned phase-matched microwave mode over the frequency range that lies within an optical resonance: only signals at $\nu = 10$ FSR = 78.83 GHz within a bandwidth of 2.45 MHz are upconverted. The generated sidebands

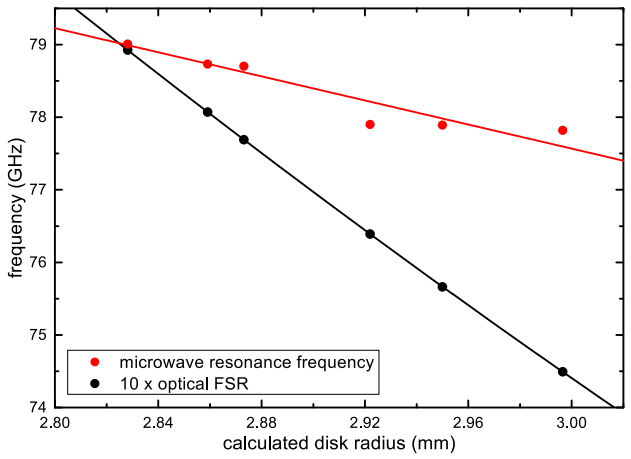

Fig. 6. Phase-matching adjustment by polishing. The resonator is polished to reduce progressively its radius. At each polishing step, the resonance frequency of the $m = 10$ microwave mode is plotted (red dots) along with the optical free spectral range of the cavity multiplied by 10 (black dots).

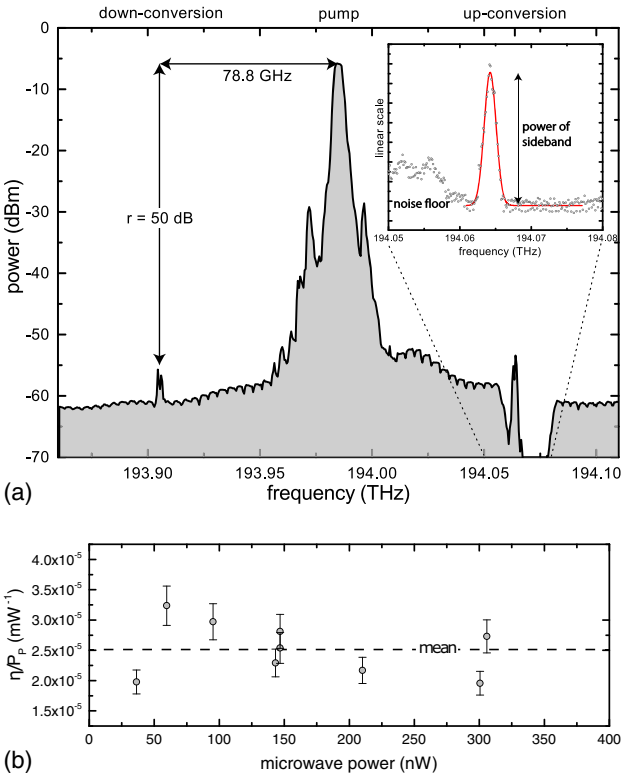

Fig. 7. (a) Spectrum of the pump and upconverted sidebands observed in the optical spectrum analyzer. In the inset the zoomed-in SFG sideband. (b) Calculation of the normalized conversion efficiency η/P_p as a function of the input microwave power, obtained from the measured power of the SFG sideband.

are then outcoupled by the same prism and detected by an optical spectrum analyzer as shown in Fig. 7(a). Amplified spontaneous emission from the pump laser's gain medium sets the noise floor of the measurement. A Bragg notch filter locally filters the pump noise around the wavelengths where the SFG sideband appears. By fixing the pump power at $P_p = 0.33$ mW, the power of the generated sidebands is measured for different values of input microwave power. From this, the normalized efficiency η/P_p is calculated taking into account the optical losses of the setup [see Fig. 7(b)], yielding on average $\eta/P_p = (2.5 \pm 0.2) \times 10^{-5}$ mW^{-1}, corresponding to a nonlinear coupling rate $g = 2\pi \times (7.7 \pm 0.3)$ Hz. To the best of our knowledge, this result surpasses the so far best reported millimeter-wave photon conversion efficiency by 2 orders of magnitude in WGM cavities [4] and by a factor of 30 in state-of-the-art ultra-wideband lithium niobate waveguide phase modulators [25]. Nevertheless, as shown in Fig. 3, conversion efficiencies on the order of $\eta \approx 10^{-2}$ or higher are needed to build room-temperature radiometers with exceptional sensitivity. This would in principle require our scheme to be effectively pumped by more than 330 mW, leading to strong instabilities due to thermorefractive and photorefractive effects in lithium niobate [26–28]. However, a better lock-in scheme and the excitation of high polar index optical modes that reduces the intracavity power density would allow us to pump with enough power to increase the efficiency further by about 2 orders of magnitude. Moreover, about 4 times better modal overlap can be achieved if the resonator is ring-shaped, increasing the nonlinear rate from Eq. (2) by one order of magnitude and, thus, yielding the required values of η. Therefore, different resonator fabrication techniques are worth investigating for this aim.

5. DISCUSSION AND CONCLUSIONS

Several characteristics of the upconverter can be improved to approach the unity conversion efficiency. First, full wave simulations show an enhancement in the efficiency of one order of magnitude if a hole is drilled in the disk. This is so because the microwave mode in such a ring-shaped resonator has a reduced volume and a higher intensity in the region of interaction with the optical mode. Moreover, since microwave losses in $LiNbO_3$ limit the intrinsic quality factor to around $Q \approx 400$, very radially narrow $LiNbO_3$ rings filled with a wider ring made of a low-losses material such as high-resistivity silicon or sapphire, as shown in Fig. 4, can provide a higher microwave Q with better modal overlap, increasing further the efficiency and reducing thermal noise due to the possibility of stronger overcoupling. The main challenge here is the fabrication of narrow (≈50–100 μm wide) $LiNbO_3$ rings [29,30]. Second, a better distribution of the pump power can be accomplished by using high polar-order optical modes. This allows more power to be pumped before the crystal becomes thermally unstable, thus increasing the efficiency. Additionally, other nonlinear crystals are worth exploring for this application due to its potential. For instance, gallium arsenide and gallium selenide exhibit stronger second-order nonlinearities and lower microwave losses than $LiNbO_3$, although no demonstration of high optical Q ($\approx 10^8$) millimeter-sized cavities has been tried yet [5]. Barium titanate exhibits an exceptionally strong second-order nonlinearity that would increase the conversion efficiency by about 3 orders of magnitude. However, barium titanate is very lossy in the millimeter-wave range compared to lithium niobate, requiring smaller resonators with strong millimeter-wave overcoupling to avoid thermal noise. Since the nonlinear parametric upconversion process is extremely broadband, one of the main advantages of this concept is its ability to be designed to work over frequencies ranging from microwaves up to terahertz. The main limitation will arise from the losses of the nonlinear materials at higher frequencies rather than in the conversion efficiency, since shorter wavelengths have better overlap with the optical mode. Nevertheless, if material losses are significantly high at terahertz frequencies, the receiver would be almost limited by background noise (300 K at room temperature) provided that the efficiency approaches unity. This would still represent a very high overall sensitivity for a room-temperature receiver at terahertz frequencies.

Owing to the highly resonant nature of the proposed upconverter, the upconversion bandwidth is limited by the bandwidth of the optical sideband, which in our experiment was about 2 MHz. Such a high spectral resolution is required in many applications such as Earth observation with hyperspectral sounders for numerical weather prediction. However, a practical radiometer usually requires a wider reception bandwidth on the order of hundreds of megahertz to have a sufficiently high overall sensitivity with reasonably low integration times. At the expense of reducing significantly the efficiency, the upconversion bandwidth of the WGM-based scheme can be increased by overcoupling the optical modes such that the resonances are broadened. However, optical couplers that are selective in frequency or polarization could broaden only the sideband while keeping the pump critically

coupled, increasing the bandwidth with lower impact in the overall conversion efficiency. By using coupled mode theory, we theoretically studied the frequency-dependent coupling strength between a lithium niobate resonator and an optical waveguide whose refractive index is periodically modulated along the propagation direction to create a Bragg grating [31]. The Bragg period Λ must satisfy $\Lambda = 2\pi(\beta_w - \beta_r)^{-1}$ at a given frequency ν_{Bragg}, where β_w and β_r are the waveguide's and resonator's propagation constants, respectively. The resulting coupling strength between copropagating waveguide and resonator modes is $|t| = |k\Delta L\text{sinc}(\gamma L)|$, where ΔL is the effective interaction length and $\gamma^2 = |k|^2 + (\Delta\beta/2)^2$ with $\Delta\beta = \beta_w - \beta_r - 2\pi/\Lambda$. $\Delta\beta$ scales with frequency as $\nu - \nu_{\text{Bragg}}$, giving t a strong frequency dependence. k is proportional to the index modulation contrast of the grating Δn and to the overlap integral between waveguide and resonator modes. To achieve a strong coupling, it might be necessary for the waveguide to cover a significant portion of the resonator's perimeter. However, it is found that the index modulation $\Delta n \approx 10^{-4}$ achievable in a UV-exposed tapered glass fiber is too low to overcouple any of the modes in the resonator, even if the fiber surrounds half of the resonator's perimeter $\Delta L = \pi R$ where R is the resonator's radius. Interestingly, increasing ΔL by using larger resonators does not help since the amplitude of the WGM's evanescent field and thus the overlap integral decay approximately with R^{-1}. On the other hand, we found that strong coupling can be accomplished with a grating-etched silicon waveguide, following the resonator's curvature over one quarter of its perimeter $\Delta L = \pi R/2$ (see inset in Fig. 8). In this case the grating has a high modulation index $\Delta n \approx 2.48$ that allows for strong overcoupling near ν_{Bragg} and weak coupling few hundreds of gigahertz away. As depicted in Fig. 8, the frequency-dependent coupling equivalent bandwidth of the structure can be exploited to critically couple the pump, while overcoupling the sideband such that upconversion of ≈130 GHz signals with about 800 MHz of bandwidth can be achieved.

Polarization-sensitive structures can be an alternative to the frequency-sensitive Bragg couplers. A birefringent coupling prism could be used in barium titanate or lithium tantalate resonators, which have a strong electro-optic coefficient for orthogonal optical modes, to significantly overcouple the TM sideband, while critically coupling the TE pump, allowing conversion bandwidths of more than 100 MHz [32,33]. On the other hand, the use of nonresonant upconverters allows for extremely large operation bandwidths [25], at the expense of yielding lower efficiencies and much higher losses than the WGM resonators due to the millimeter-wave confinement with metallic structures. This hinders the use of such electro-optic modulators as room-temperature low noise millimeter-wave receivers since the effective temperature is fixed to $T_{\text{eff}} \approx 300$ K while η is still far from unity.

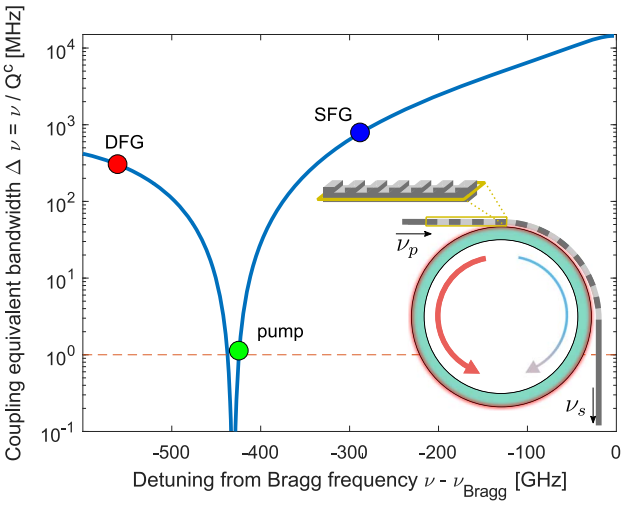

Fig. 8. Theoretical frequency-selective coupling bandwidth $\Delta\nu = \nu/Q^c$ (Q^c being the mode's coupling Q factor) between each optical WGM and a silicon waveguide where a Bragg grating is etched. Upconversion of ≈130 GHz signals to the SFG sideband with ≈800 MHz of bandwidth is possible.

Even though a SFG single sideband upconversion is free of spontaneous parametric down conversion noise, the generation of both SFG and DFG sidebands inside a WGM upconverter is naturally easier to achieve due to the uniformity of the cavity's free spectral range. DFG generation produces optical amplification of the signal [7], which may be exploited to surpass the dark count noise of the photodetectors in a narrowband radiometer. We estimate the SPDC noise generated in a dual sideband upconverter to have an equivalent temperature of 4.9 K and 10.1 K for 94 GHz and 180 GHz, respectively. Depending on the effective thermal noise temperature T_{eff} of the upconverter, this might be considered a low noise contribution for a room-temperature radiometer.

It is worth investigating a heterodyne scheme for optical detection due to its potential sensitivity benefits. The laser pump can be modulated in a single-sideband modulator driven by a millimeter-wave local oscillator at a frequency close to the detection frequency. The resulting sideband is then coupled to one input of the beamsplitter at one of the upconverter's output (see Fig. 2). The antenna temperature can then be retrieved by postprocessing the signals of the balanced photodetectors. The effects of laser phase noise and linewidth for this scheme have to be studied.

Funding. Ministerio de Economía y Competitividad (MINECO) (TEC2013-47753-C3); Comunidad de Madrid (S2013/ICE-3004); Banco Santander (TEC2016-76997-C3-2-R); Banco Bilbao Vizcaya Argentaria (BBVA) (IN[16]_TIC_TIC_0040); 2017 UC3M-Santander Chair of Excellence.

†These authors contributed equally to this work.

REFERENCES

1. PRISM collaboration, "Prism (polarized radiation imaging and spectroscopy mission): an extended white paper," J. Cosmol. Astropart. Phys. **2014**, 006 (2014).
2. A. R. Cooray and Origins Space Telescope Study Team, "Origins space telescope," in *American Astronomical Society Meeting Abstracts* (2017), Vol. **229**, pp. 405.01.
3. J. R. Goicoechea, K. Isaak, and B. Swinyard, "Exoplanet research with SAFARI: a far-IR imaging spectrometer for SPICA," arXiv: 1002.2861v1 (2009).
4. D. V. Strekalov, A. A. Savchenkov, A. B. Matsko, and N. Yu, "Efficient upconversion of subterahertz radiation in a high-Q whispering gallery resonator," Opt. Lett. **34**, 713–715 (2009).
5. D. V. Strekalov, C. Marquardt, A. B. Matsko, H. G. L. Schwefel, and G. Leuchs, "Nonlinear and quantum optics with whispering gallery resonators," J. Opt. **18**, 123002 (2016).
6. A. Rueda, F. Sedlmeir, M. C. Collodo, U. Vogl, B. Stiller, G. Schunk, D. V. Strekalov, C. Marquardt, J. M. Fink, O. Painter, G. Leuchs, and H. G. L. Schwefel, "Efficient microwave to optical photon conversion: an electro-optical realization," Optica **3**, 597–604 (2016).

7. D. N. Klyshko, *Photons and Nonlinear Optics* (CRC Press, 1988).
8. V. V. Kornienko, G. K. Kitaeva, F. Sedlmeir, G. Leuchs, and H. G. L. Schwefel, "Towards terahertz detection and calibration through spontaneous parametric down-conversion in the terahertz idler-frequency range generated by a 795 nm diode laser system," APL Photon. **3**, 051704 (2018).
9. P. Powers and J. Haus, *Fundamentals of Nonlinear Optics* (Electro-Optics and Photonics Faculty, 2017).
10. D. V. Strekalov, H. G. L. Schwefel, A. A. Savchenkov, A. B. Matsko, L. J. Wang, and N. Yu, "Microwave whispering-gallery resonator for efficient optical upconversion," Phys. Rev. A **80**, 033810 (2009).
11. A. Matsko, D. Strekalov, and N. Yu, "Sensitivity of terahertz photonic receivers," Phys. Rev. A **77**, 043812 (2008).
12. J. D. Kraus, *Radio Astronomy* (McGraw-Hill, 1966).
13. A. Yariv, "Universal relations for coupling of optical power between microresonators and dielectric waveguides," Electron. Lett. **36**, 321–322 (2000).
14. H. A. Haus, "Thermal noise in dissipative media," J. Appl. Phys. **32**, 493–500 (1961).
15. L. Rodney, *The Quantum Theory of Light* (Oxford, 1973).
16. L. Mandel, "Fluctuations of photon beams: the distribution of the photo-electrons," Proc. Phys. Soc. **74**, 233–243 (1959).
17. P. Darré, R. Baudoin, J.-T. Gomes, N. J. Scott, L. Delage, L. Grossard, J. Sturmann, C. Farrington, F. Reynaud, and T. A. T. Brummelaar, "First on-sky fringes with an upconversion interferometer tested on a telescope array," Phys. Rev. Lett. **117**, 233902 (2016).
18. R. W. Boyd, "Infrared upconversion for astronomy," Opt. Eng. **16**, 166563 (1977).
19. M. Born, E. Wolf, A. B. Bhatia, P. C. Clemmow, D. Gabor, A. R. Stokes, A. M. Taylor, P. A. Wayman, and W. L. Wilcock, *Principles of Optics: Electromagnetic Theory of Propagation, Interference and Diffraction of Light*, 7th ed. (Cambridge University, 1999).
20. N. Jarosik, C. L. Bennett, M. Halpern, G. Hinshaw, A. Kogut, M. Limon, S. S. Meyer, L. Page, M. Pospieszalski, D. N. Spergel, G. S. Tucker, D. T. Wilkinson, E. Wollack, E. L. Wright, and Z. Zhang, "Design, implementation, and testing of the microwave anisotropy probe radiometers," Astrophys. J. **145**, 413–436 (2003).
21. P. Kangaslahti, B. Lim, T. Gaier, A. Tanner, M. Varonen, L. Samoska, S. Brown, B. Lambrigtsen, S. Reising, J. Tanabe, O. Montes, D. Dawson, and C. Parashare, "Low noise amplifier receivers for millimeter wave atmospheric remote sensing," in *IEEE/MTT-S International Microwave Symposium Digest* (2012), pp. 1–3.
22. S. Preu, F. H. Renner, S. Malzer, G. H. Döhler, L. J. Wang, M. Hanson, A. C. Gossard, T. L. J. Wilkinson, and E. R. Brown, "Efficient terahertz emission from ballistic transport enhanced n-i-p-n-i-p superlattice photomixers," Appl. Phys. Lett. **90**, 212115 (2007).
23. A. Rivera-Lavado, S. Preu, L. Garcia-Munoz, A. Generalov, J. Montero-de Paz, G. Dohler, D. Lioubtchenko, M. Mendez-Aller, F. Sedlmeir, M. Schneidereit, H. Schwefel, S. Malzer, D. Segovia-Vargas, and A. Raisanen, "Dielectric rod waveguide antenna as THz emitter for photomixing devices," IEEE Trans. Antennas Propag. **63**, 882–890 (2015).
24. I. Breunig, B. Sturman, F. Sedlmeir, H. G. L. Schwefel, and K. Buse, "Whispering gallery modes at the rim of an axisymmetric optical resonator: analytical versus numerical description and comparison with experiment," Opt. Express **21**, 30683–30692 (2013).
25. A. J. Mercante, S. Shi, P. Yao, L. Xie, R. M. Weikle, and D. W. Prather, "Thin film lithium niobate electro-optic modulator with terahertz operating bandwidth," Opt. Express **26**, 14810–14816 (2018).
26. M. Leidinger, C. S. Werner, W. Yoshiki, K. Buse, and I. Breunig, "Impact of the photorefractive and pyroelectric-electro-optic effect in lithium niobate on whispering-gallery modes," Opt. Lett. **41**, 5474–5477 (2016).
27. A. E. Fomin, M. L. Gorodetsky, I. S. Grudinin, and V. S. Ilchenko, "Nonstationary nonlinear effects in optical microspheres," J. Opt. Soc. Am. B **22**, 459–465 (2004).
28. A. A. Savchenkov, A. B. Matsko, D. Strekalov, V. S. Ilchenko, and L. Maleki, "Enhancement of photorefraction in whispering gallery mode resonators," Phys. Rev. B **74**, 245119 (2006).
29. R. Wolf, I. Breunig, H. Zappe, and K. Buse, "Cascaded second-order optical nonlinearities in on-chip micro rings," Opt. Express **25**, 29927–29933 (2017).
30. L. Chen, Q. Xu, M. G. Wood, and R. M. Reano, "Hybrid silicon and lithium niobate electro-optical ring modulator," Optica **1**, 112–118 (2014).
31. A. Yariv and M. Nakamura, "Periodic structures for integrated optics," IEEE J. Quantum Electron. **13**, 233–253 (1977).
32. F. Sedlmeir, M. R. Foreman, U. Vogl, R. Zeltner, G. Schunk, D. V. Strekalov, C. Marquardt, G. Leuchs, and H. G. L. Schwefel, "Polarization-selective out-coupling of whispering-gallery modes," Phys. Rev. Appl. **7**, 024029 (2017).
33. L. S. Trainor, F. Sedlmeir, C. Peuntinger, and H. G. Schwefel, "Selective coupling enhances harmonic generation of whispering-gallery modes," Phys. Rev. Appl. **9**, 024007 (2018).